0026-895X/99/020633-11$3.00/0

MOLECULAR PHARMACOLOGY, **56:**633–643 (1999).

Molecular Modeling of the Intrastrand Guanine-Guanine DNA Adducts Produced by Cisplatin and Oxaliplatin

ERIC D. SCHEEFF,[1] JAMES M. BRIGGS,[2] and STEPHEN B. HOWELL

Department of Medicine and Cancer Center (E.D.S., S.B.H.), and Department of Pharmacology (J.M.B.), University of California, San Diego, La Jolla, California

Received January 11, 1999; accepted May 7, 1999

This paper is available online at http://www.molpharm.org

ABSTRACT

Intrastrand DNA adducts formed by cisplatin and oxaliplatin were modeled with molecular mechanics minimization and restrained molecular dynamics simulations in a comparative study. A reasonable set of force field parameters for the Pt atom were refined by using the available cisplatinated DNA crystal structure as a guide. This crystal structure was also used as the starting structure for the simulations. Analysis of the resulting structures indicated that the covalent effects of oxaliplatin coordination on DNA structure were very similar to those of cisplatin. The most prominent difference between the two structures resulted from the presence of the 1,2-diaminocyclohexane ring in the oxaliplatin adduct. The modeling indicated that this ring protrudes directly outward into, and fills much of, the narrowed major groove of the bound DNA, forming a markedly altered and less polar major groove in the area of the adduct. The differences in the structure of the adducts produced by cisplatin and oxaliplatin are consistent with the observation that they are differentially recognized by the DNA mismatch repair system.

It is generally accepted that the primary cytotoxic mode of action of cisplatin is the production of adducts in DNA. The most prevalent adduct is the intrastrand linkage of two adjacent guanine bases by the nitrogen atoms at position 7 (the GG adduct). Experimentally derived structures for the cisplatin GG adduct in double-stranded DNA are available in the form of an octamer duplex solved by NMR (Yang et al., 1995) and a dodecamer duplex solved by crystallography (Takahara et al., 1996a,b) and NMR (Gelasco and Lippard, 1998). The three structures display a notable bend toward the major groove in the double helix of 35–78°, which varies depending on the structure and the particular method of measurement used. This bend produces a narrowing of the major groove and a broadening and flattening of the minor groove similar to that seen in A-DNA. Furthermore, the crystal structure assumes a more A-DNA-like conformation on one end of the molecule and a more B-DNA-like conformation on the other, although this was not observed in the NMR structures and may be a product of crystal packing forces (Gelasco and Lippard, 1998).

Oxaliplatin [1*R*,2*R*-diaminocyclohexane platinum (II) oxalate], a platinum compound now in clinical development (Raymond et al., 1998), differs from cisplatin by the addition of a cyclohexane ring to the ammines of cisplatin to form a diaminocyclohexane (DACH) ring (Fig. 1). Although the post-biotransformation leaving groups of these compounds are apparently the same (Raymond et al., 1998), and it has been shown that oxaliplatin has a similar adduct formation profile to that of cisplatin (Saris et al., 1996; Woynarowski et al., 1998), one would anticipate the GG adduct to be structurally dissimilar once the drugs are bound to DNA.

It is now known that components of the DNA mismatch repair (MMR) system bind to the cisplatin GG adduct (Mello et al., 1996; Yamada et al., 1997) and, by an undetermined mechanism, promote cellular apoptosis. Thus, cells that lack a functional MMR system are more resistant to cisplatin injury (Fink et al., 1996). The MMR system may enhance cisplatin sensitivity through the shielding of adducts from appropriate repair, direct signaling to the apoptotic machinery, or the initiation of a futile cycle of attempted repair that eventually produces lethal DNA strand breaks. In contrast, the loss of functional MMR does not confer resistance to oxaliplatin (Fink et al., 1996). Thus, oxaliplatin adducts apparently are not recognized or processed by the MMR system in the same way as cisplatin adducts. The structural basis for

This work was supported by a search contract from Sanofi Research (Malvern, PA). This work was conducted in part by Clayton Foundation for Research—California Division. Dr. Howell is a Clayton Foundation investigator. A preliminary account of this work was presented at the 1998 Annual Meeting of the American Association for Cancer Research [Abstract no. 1082, *Proc Am Assoc Cancer Res* **39:**158]

[1] Present address: San Diego Supercomputer Center 0537, University of California, San Diego, La Jolla, California.

[2] Present address: Department of Biology and Biochemistry, University of Houston, Houston, Texas.

ABBREVIATIONS: DACH, diaminocyclohexane; AMBER, assisted model building with energy refinement; MD, molecular dynamics; MMR, DNA mismatch repair; PDB, Protein Data Bank; RMS, root mean squared.

the lack of oxaliplatin recognition is unclear and could involve direct steric hindrance by the DACH ring or a distortion in DNA that is distinct from that produced by cisplatin. Only limited information is available on the structure of hMSH2 (De las Alas et al., 1998), the primary DNA binding protein of the MMR system, and no structural information is available on the other human MMR proteins. However, data is available for the homologous system in bacteria that suggests that the MMR proteins contact mismatches at multiple sites, both at the point of the mismatch and at other atoms up and down the major and minor grooves (Biswas and Hsieh, 1997).

An experimentally derived structure does not exist for the oxaliplatin GG adduct. Therefore, we sought to determine a likely structure for the oxaliplatin adduct to provide insight into the structural features that might account for differential recognition by the MMR system. We used molecular mechanics minimization and restrained molecular dynamics to develop a model of the cisplatin and oxaliplatin GG adducts by using the known crystal structure of the cisplatin adduct as a guide. A forcefield was developed that contained a refined set of parameters for the unusual presence of platinum in the molecule, and this field was tested against the crystal structure. The oxaliplatin adduct in a double-stranded DNA molecule was produced through modification of the cisplatin crystal structure. The modeled cisplatin and oxaliplatin adducts were then put through identical energy minimization and molecular dynamics simulations, and the resulting molecules compared to determine the likely effect of the presence of the DACH ring of oxaliplatin on the adduct and overall DNA structure.

An in vacuo modeling environment with implicit consideration of solvent and some atomic constraints (during dynamics simulations) was used. This methodology made the computation times tractable during the multiple, repetitive simulations required in this study. These were particularly important for the critical development and testing of a broad range of potential parameters for the platinum atom. Newer methodologies exist that consider solvent atoms and counterions explicitly, use the particle mesh Ewald summation for the treatment of boundary conditions, do not require atomic constraints, and have been shown to produce more accurate DNA structures than the methods used here (Young et al., 1997; Duan et al., 1997). However, the extremely high central processing unit demands and run times of these methods precluded their use in this study, and the reader is therefore cautioned to take note of this limitation. Implicit solvent techniques have been suggested to provide acceptable accuracy for DNA modeling (Falsafi and Reich, 1993; Kozack and Loechler, 1997), and this initial work provides a foundation for the eventual exploration of strained, platinated DNA molecules with the advanced full solvent techniques mentioned above.

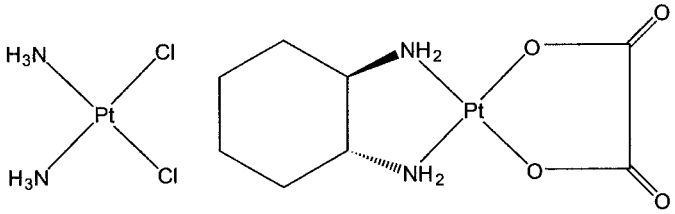

Fig. 1. Cisplatin and oxaliplatin molecules before DNA binding. Chemical groups to the right of the Pt are removed during biotransformation, and both drugs bind to DNA directly via the Pt atom. Two nitrogen-bound cyclohexane carbons are both in the *R* configuration in oxaliplatin.

Materials and Methods

Computing. All modeling was performed on a Silicon Graphics workstation with the InsightII (95.0) and (97.0) software suites (Molecular Simulations Inc., San Diego). Molecular mechanics and dynamics simulations were performed with the Discover module of this package. The assisted model building with energy refinement (AMBER) force field (Weiner et al., 1984; equation given below), as provided with InsightII (95.0), was used with specific modifications for the presence of a platinum atom as discussed below. Analysis of the resultant structures was performed with the Analysis module of InsightII.

AMBER Equation. The AMBER equation used was as follows.

$$E_{total} = \sum K_r(r - r_0)^2(\text{bond stretch}) + \sum K_\theta(\theta - \theta_0)^2(\text{angle bend}) + \sum V_n[1 + \cos(n\varphi - \varphi_{0n})](\text{torsions}) + \sum V\{1 + \cos(n\chi - \chi_0)\}(\text{improper torsions}) + \sum \varepsilon[(r_{ij}^*/r_{ij})^{12} - 2(r_{ij}^*/r_{ij})^6](\text{van der Waals}) + \sum [A_{ij}/r_{ij}^{12} - B_{ij}/r_{ij}^{10}](\text{H-bonding}) + \sum (q_i q_j)/\varepsilon_{ij} r_{ij}(\text{electrostatic})$$

Starting Structure. The structure on which the modeling effort was based was the available crystal structure (Takahara et al., 1996a,b) for the cisplatinated DNA dodecamer d[CCTCTG*G*TCTCC]/d[GGAGACCAGAGG], where G* denotes an adducted base. This structure was downloaded from the Protein Data Bank (PDB; Bernstein et al., 1977; www.pdb.bnl.gov/www.rcsb.org; PDB code 1AIO) and modified for use in this study. As the PDB file contains two very similar molecules (one unit cell), we selected the first of the two in the PDB file for use in our study. We adopted the identical base numbering pattern (for referring to particular nucleotides) as was used in the PDB file and by Takahara et al. (1996a,b).

Hydrogens were added to the structure with the hydrogen addition function available in the InsightII Biopolymer interface. This function provided hydrogen placement that produced very reasonable nucleotide structures. Therefore, the hydrogens were not subjected to any form of optimization after addition to the molecule used in the simulation.

Base 3 in the crystal structure had been substituted in the form of an isomorphous replacement of 5-bromouridine for thymine. As our goal was to model the DNA adducts as they would exist in cells, we chose to modify this base back to a thymine by replacing the bromine atom with a methyl group. This structure was used as the starting point for all cisplatin simulations, and all comparisons made against the "crystal structure" in this article were made to this slightly modified version.

To produce a starting structure for the oxaliplatin GG adduct, a cyclohexane molecule was bound to the ammine groups of cisplatin via two adjacent carbon atoms in the ring such that these chiral carbons were both in the *R* configuration. The modification was performed through the Builder module of InsightII, and effectively reproduced the DACH structure of oxaliplatin. To optimize the bonds of the artificially attached ring, the cyclohexane residue was subjected to conjugate gradient minimization until convergence (a maximum derivative <0.001 kcal mol^{-1}Å^{-1}) with the rest of the molecule fixed. All comparisons made to the "starting structure" of oxaliplatin refer to this structure. It should be noted that at the beginning of the

simulations, the oxaliplatin and cisplatin adduct structures were completely identical, with the exception of the added cyclohexane ring of the oxaliplatin structure.

Forcefield Parameterization. Because cisplatin and oxaliplatin contain a platinum atom, for which the standard AMBER forcefield does not include parameters, it was necessary to develop a modified version of the field that included appropriate values. A set of forcefield parameters and partial charges has been proposed by Yao et al. (1994). These parameters integrated a variety of experimental data and previous molecular modeling studies, and the authors were able to demonstrate agreement with both NMR and crystallographic data of cisplatin bound to several small guanine base structures. However, this study was completed before the availability of the full-length, double-stranded NMR (Yang et al., 1995; Gelasco and Lippard, 1998) and crystal (Takahara et al., 1996a,b) structures now available. It was deemed reasonable to test these parameters against the double-stranded crystal structure and make minor modifications if necessary to enhance agreement.

Evaluation of the values suggested by Yao et al. (1994) was conducted as follows. The values were entered into the AMBER forcefield as described below. Exploratory energy minimization of the modified cisplatin crystal structure was then initiated in vacuo for 500 steps of steepest descent and 3000 steps of conjugate gradient minimization. A distance-dependent dielectric of $\epsilon = 4r_{ij}$ was used to mimic solvent effects, an arrangement that has been successfully used in previous studies (Orozco et al., 1990; Yao et al., 1994). The 1–4 van der Waals terms were also scaled by a factor of 0.5, as suggested (Discover 95.0 Manual; Yao et al., 1994). For this simulation, we chose to lower the charges on the phosphate groups such that each nucleotide had a net charge of -0.2, according to the method described by Veal and Wilson (1991). This charge reduction mimics the effects of the counterion condensation that occurs around DNA in solution. As suggested (Veal and Wilson, 1991; Yao et al, 1994), we did not reduce the charges on nucleotides bound to cisplatin, so as to represent the release of counterions on the binding of this cationic ligand.

The molecules that resulted from the above minimization procedure were superimposed on the crystal structure and compared. Bond stretching and nonbonded parameters were retained unchanged from the suggested values. Angle bending and torsional and improper torsional terms were systematically altered to test for enhanced agreement with the crystal structure. This was done by both raising and lowering the force constant for the energy term in question and rerunning the above simulation. If either an increase or decrease in the force constant enhanced agreement with the crystal structure, further modification in the direction suggested was tested. If there was ambiguity as to the benefits of a particular change, the initial value from Yao et al. (1994) was favored. The most promising parameter combinations were subjected to another 3000 iterations of conjugate gradients minimization and then reevaluated. In the end, it was found that the suggested parameters (Yao et al., 1994) produced excellent agreement with the crystal structure, provided a few minor modifications were made to them.

We adopted the same specialized atom types as Yao et al. (1994; Fig. 2; Table 1): N31 and N32 for the two ammine/amine nitrogens, NB1 and NB2 for Pt-bound guanine nitrogens, and PT for the central Pt atom. The ammine/amine hydrogens were treated as standard H3 hydrogens. Our postevaluation force constants for these atoms are listed in Table 1. Aside from the values explicitly listed, N31/N32 (referred to as N3X) and NB1/NB2 (referred to as NBX) were parameterized throughout the forcefield identically to the standard AMBER atom types N3 and NB, respectively.

Charges for the specialized atom types and the bound guanine groups were arranged exactly as suggested (Yao et al., 1994; Figs. 3 and 4; Table 2), as were the values for bond stretching. The suggested values for angle bend deformation were used, with one exception: Yao et al. (1994) had suggested that the CB-NB/NBX-CK bond be adjusted to 104.1° from the standard value of 103.8°. The bond angles given in the crystal structure were closer to the 103.8° value, and as our intent was to model the crystal structure as closely as possible, the standard value was retained. Yao et al. (1994) did not provide an angle or force constant for the PT-N3X-H3 bond, so we treated PT as an sp3 carbon (CT) to achieve an angle of 109.5° and force constant of 35 kcal mol^{-1} rad^{-2} (Table 1).

The values for torsional deformation suggested by Yao et al. (1994) were expanded and modified slightly. Although the authors provided values for most of the torsions involving NBX, PT, and N3X, they did not suggest values for CB/CK-NB2-PT-N32 and CB/CK-NB1-PT-N31. It was reasoned that the considerable torsional values already suggested for these atoms, although in different combinations of bonds, would be sufficient for the assumption of the proper structure, and that further values would be redundant. Furthermore, torsions about these bonds would most likely have a very low resistance because of the nearly linear nature of the NB2-PT-N32 and NB1-PT-N31 bonds (Fig. 2) Therefore, the torsions for the above groups were given a force constant of 0.

Yao et al. (1994) also did not suggest torsional parameters for rotations around the PT-N3X bond. As above, we used the CT atom type as a stand-in for PT. Rotations around the CT-N3 bond are treated in the standard AMBER field (Weiner et al., 1984) with a *-CT-N3-* term, where * denotes any atom. This arrangement was duplicated with a *-PT-N3X-* term, with a periodicity of 3 and a force constant of 1.40 kcal mol^{-1} (Table 1).

Torsions without platinum as a central atom also required adjustment. In the normal AMBER field, torsions with the atoms CB-NB at the center are arranged with the term *-CB-NB-*, where * denotes any atom. This "wildcard" term is assigned a high force constant, with a ϕ angle of 180°, which promotes planarity of the base. If the torsions for NBX were simply copied from this arrangement, the result was terms such as C-CB-NBX-PT and CB-CB-NBX-PT with extremely high planar force constants. On exploratory energy minimization, a severe pucker of the base in the direction of the platinum atom occurred as the molecule strained to achieve planarity. An identical situation existed for *-CK-NBX-*. In both cases, it was found that setting the torsional force constants to 0 (where PT was involved) corrected the problem. However, the planar geometry of the base was somewhat destabilized, so it was decided to retain a CB-CB-NBX-PT force constant of 5 kcal/mol (Table 1).

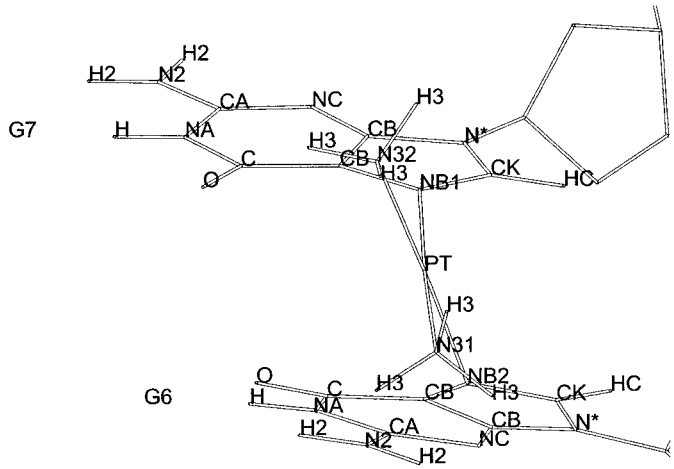

Fig. 2. MOLSCRIPT (Kraulis, 1991) image depicting the atom potential types used in modeling the GG adducts. The view faces the major groove and is a close-up of the two bound guanines and the cisplatin adduct (partner strand cytosines are not shown). The image has a similar overall orientation to that described for Fig. 5. Hydrogens are only shown for the cisplatin adduct and two adducted guanines. Oxaliplatin adducts were arranged with identical atom types to those shown, except that one H3 atom on both N31 and N32 was replaced by a CT atom of the cyclohexane ring.

Yao et al. (1994) also included an improper torsional value in their forcefield to help prevent base plane pucker, and our evaluation suggested that this term was very helpful in achieving that result. As such, it was included in our forcefield.

After 500 steepest descent and 6000 conjugate gradient minimization steps, the listed parameter set (Tables 1 and 2) produced reasonable agreement with the crystal structure, with a heavy atom root mean squared (RMS) deviation of 0.84Å. If only the platinum, ammine nitrogens, and heavy atoms of the two bound guanine bases were considered, the RMS deviation was 0.34Å, a value close to that achieved in similar measurements of complexes in Yao et al. (1994). These parameters were used for the remainder of the study.

Oxaliplatin Parameterization. A small number of additional parameters were necessary for the oxaliplatin adduct as a result of the presence of the cyclohexane ring in this compound. The standard AMBER atom types of CT for the carbons and HC for the hydrogens were used for the cyclohexane ring. As with the cisplatin parameterization, many of the parameters for interaction of N3X with the cyclohexane ring were arranged through the use of the standard AMBER parameters for N3. This method was sufficient for parameterization of all interactions not involving the PT atom, and therefore explicit values are not listed in Table 1.

Only one additional parameterization was required that involved the platinum atom, and once again modified forms of the parameters for the CT atom type were used to determine values for PT. For the CT-N3X-PT bond angle deformation, an angle of 109.5° (the same as that for H3-N3X-PT) was chosen to promote a tetrahedral geometry around the N3X atoms. However, the CT-N3-CT force constant of 50 kcal mol^{-1} rad^{-2} was used to reflect the presence of CT (as opposed to H3) in the CT-N3X-PT angle group.

TABLE 1
Atom potential types and force constants used in modeling the cisplatin and oxaliplatin adducts
Positions of atom types shown in Fig. 2.

Atom	Description
New Atom Types[a]	
PT	Platinum atom
NB1	Nitrogen at position 7 in guanine ring, bound to PT
NB2	Nitrogen at position 7 in adjacent guanine, bound to PT, *cis* to NB1
N31	Ammine/amine nitrogen, trans to NB1 and *cis* to NB2
N32	Ammine/amine nitrogen, trans to NB2 and *cis* to NB1

Bond	r_0	K_r
	Å	*kcal mol^{-1} Å^{-2}*
Bond Stretch[a]		
PT-NB1/NB2	2.01	366
PT-N31/N32	2.03	366

Angle	θ_0	K_θ
	degree	*kcal mol^{-1} rad^{-2}*
Angle Bend		
CB-NB1/NB2-PT[a]	127.95	20
CK-NB1/NB2-PT[a]	127.95	20
NB1-PT-NB2[a]	90	42
N31-PT-N32[a]	90	42
N31-PT-NB2[a]	90	42
N32-PT-NB1[a]	90	42
N31-PT-NB1[a]	180	42
N32-PT-NB2[a]	180	42
PT-N31/N32-CT[b,c]	109.5	50
PT-N31/N32-H3[b]	109.5	35

Torsional Angle	φ_{0n}	n	V_n
			kcal mol^{-1}
Torsions			
CB/CK-NB1-PT-N32[a]	90	2	0.5
CB/CK-NB2-PT-N31[a]	90	2	0.5
CB/CK-NB1-PT-NB2[a]	90	2	0.5
CB/CK-NB2-PT-NB1[a]	90	2	0.5
CB/CK-NB2-PT-N32[b]	0	2	0
CB/CK-NB1-PT-N31[b]	0	2	0
C-CB-NB1/NB2-CK[d]	180	2	5.1
CB-CB-NB1/NB2-CK[d]	180	2	5.1
C-CB-NB1/NB2-PT[b]	180	2	0
CB-CB-NB1/NB2-PT[b]	180	2	5.0
HC-CK-NB1/NB2-CB[d]	180	2	20.0
N*-CK-NB1/NB2-CB[d]	180	2	20.0
HC-CK-NB1/NB2-PT[b]	180	2	0
N*-CK-NB1/NB2-PT[b]	180	2	0
-PT-N31/N32-[b,e]	0	3	1.4

Improper Angle	x_0	n	K_x
			kcal mol^{-1}
Improper Torsions[a]			
CK-NB1/NB2-CB-PT	180	1	10

Atom Type	r (Å)	ε
		kcal mol^{-1}
Nonbonded Interactions[a]		
PT	4.88	0.4
NB1/NB2	3.80	0.12
N31/N32	3.70	0.08

[a] Yao et al. (1994).
[b] This study.
[c] Necessary for oxaliplatin.
[d] Arranged following standard AMBER values for the NB atom type (shown for clarity).
[e] "*" Denotes any atom.

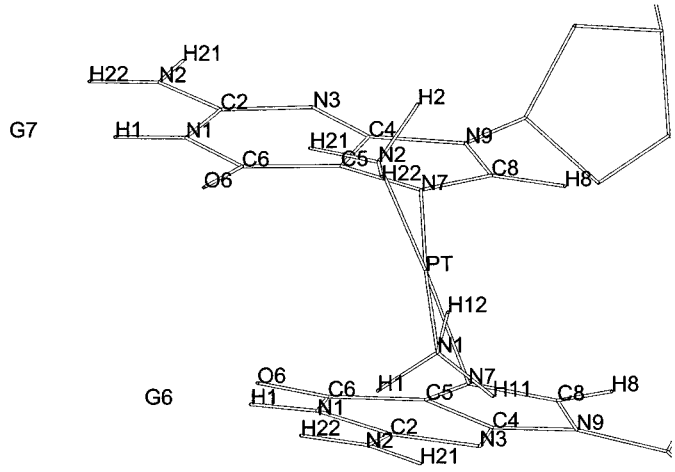

Fig. 3. MOLSCRIPT (Kraulis, 1991) image depicting the names for atoms in the cisplatin adduct and bound guanines. The orientation is identical with that in Fig. 2. Atoms in the oxaliplatin adducts were similar, except that H22 and H12 were replaced by the cyclohexane carbons.

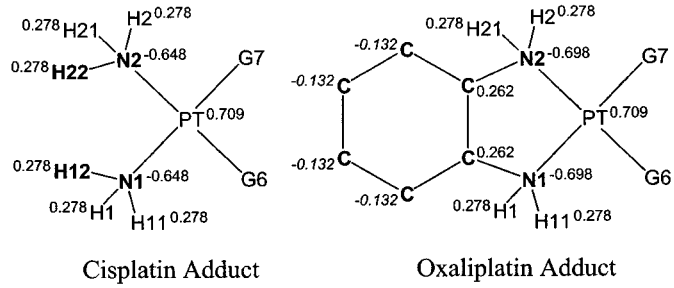

Fig. 4. Two-dimensional drawing of the adducts depicting partial charge assignments used for each by atom name. Charge values and their sources are also provided in Table 2 and explained in the text. Atoms shown in bold differed between the two adducts in charge value or in presence/absence. Charges shown in italics are unchanged from the standard AMBER values. Hydrogens are not shown for the cyclohexane ring of oxaliplatin (all had the same partial charge, as provided in Table 2). G7 and G6 refer to the bound guanine bases. Charges for these were arranged identically for the two adducts and are listed in Table 2.

Charges for the oxaliplatin adduct also had to be developed, and they were obtained from those used for the cisplatin adduct, with the exception of the charges on the N3X atoms. It was necessary to adjust the charges on these atoms to reflect attachment to the two CT atoms of cyclohexane as opposed to H3 hydrogens. To estimate the appropriate charge shift, the Pt atom was substituted with a carbon, and the automatic forcefield charge assignments were examined for the ammine nitrogens, a cyclohexane ring, and amine nitrogens bound to cyclohexane to produce a pseudo "oxaliplatin" molecule. The AMBER field did not have a full set of built-in charge assignments for this interaction, so the consistent valence force field available through the InsightII interface was used. The relative charge shifts observed were adapted to the actual oxaliplatin adduct, based on the cisplatin charges provided by Yao et al. (1994), and the cyclohexane charges as assigned by AMBER. The resultant oxaliplatin charges are provided in Table 2 and Fig. 4. The partial positive charge residing on hydrogens in the unbound molecules (a total of +0.344) was relocated to the amine-bound CT atom, which previously retained a partial charge of −0.132. An additional charge of −0.05 was also withdrawn from CT by N3X, resulting in a final CT charge of +0.262 and a final N3X charge of −0.698.

TABLE 2

Partial charges on cisplatin, oxaliplatin, bound guanines, and phosphates by atom name

Positions of named atoms shown in Figs. 3 and 4.

Atom Name	Unbound charges[a]	Platinated charges
Partial charges on guanine base		
N1	−0.729	−0.729
H1	0.336	0.336
C2	0.871	0.871
N2	−0.778	−0.778
H21	0.325	0.325
H22	0.339	0.339
N3	−0.709	−0.709
C4	0.391	0.414[b]
C5	−0.060	0.009[b]
C6	0.690	0.713[b]
O6	−0.458	−0.458
N7	−0.543	−0.314[b]
C8	0.162	0.335[b]
H8	0.150	0.069[b]
N9	−0.042	−0.019[b]

Atom Name	Charge
Partial charges on cisplatin adduct	
PT	0.709[b]
N[c]	−0.648[b]
H[d]	0.278[b]

Atom Name	Unbound Charge	Amine-Bound Charge
Partial charges on oxaliplatin adduct		
Cyclohexane charges		
C	−0.132[e]	0.262[g]
H	0.066[f]	
Amine and platinum charges		
PT	0.709[b]	
N[h]	−0.698[j]	
H[i]	0.278[b]	

Atom	Nucleotide Charge of −0.2	Nucleotide Charge of −0.6
Phosphate Charges[k]		
P	1.357	1.371
O1/O2	−0.490	−0.668
O3/O5	−0.452	−0.481

[a] Standard AMBER charges for the guanine base.
[b] From Yao et al. (1994).
[c] Named "N2" and "N1" in Figs. 3 and 4.
[d] Named "H1, H11, H12, H2, H21, and H22" in Figs. 3 and 4.
[e] AMBER charge for carbon in cyclohexane ring, used for all carbon atoms in DACH ring not bound directly to amine nitrogen.
[f] AMBER charge for hydrogen in cyclohexane ring, used for all hydrogens in cyclohexane residue of oxaliplatin adduct.
[g] This study, used only for two nitrogen-bound carbons in DACH.
[h] Atoms in same position as "N2" and "N1" of cisplatin in Figs. 3 and 4.
[i] Atoms in same position as "H2, H21, H1, and H11" in Figs. 3 and 4 (in oxaliplatin, "H22" and "H12" are replaced by cyclohexane carbons).
[j] This study.
[k] From Veal and Wilson (1991).

Simulations. This study consisted of both energy minimization and molecular dynamics simulations. In both cases, the aim was to establish valid simulation conditions by ensuring agreement of the modeled cisplatin adduct structure with that of the crystal structure. Once the conditions were validated, they were applied to the oxaliplatin adduct.

Energy Minimization. Energy minimization of the parameterized molecules was performed in vacuo with the same dielectric and 1–4 nonbond adjustments as described above. The phosphate charges were reduced to −0.2 per nucleotide to account for counterion condensation. Both adducted DNA molecules were minimized for 500 steepest descent and 6000 conjugate gradient steps, at which point the structures had RMS derivatives of ~0.03 kcal $mol^{-1}Å^{-1}$ for cisplatin and ~0.008 kcal $mol^{-1}Å^{-1}$ for oxaliplatin. The energy-minimized cisplatin adduct retained a structure very similar to the crystal structure (heavy atom RMS deviation for the whole molecule was 0.84Å). However, the oxaliplatin-adducted DNA exhibited multiple structural deviations, most notably, severe narrowing of the major groove and broadening of the minor groove. Although these differences suggested an alternate overall DNA structure for the oxaliplatin adduct (Scheeff and Howell, 1998), severe narrowing of the major groove requires tight packing of the phosphate groups, a configuration that seemed unlikely.

Exploratory molecular dynamics trajectories of the cisplatin adduct displayed a rapid and irreversible narrowing of the major groove similar to that seen in the energy-minimized oxaliplatin structure. As this groove narrowing is inconsistent with the crystal structure, it was concluded that this was most likely an artifact of our phosphate charge-reduction scheme. Presumably, lowering the charges on the phosphate groups to −0.2 provides an insufficient repulsive force to prevent the close packing of the phosphates in a bent DNA molecule, leading to collapse of the structure. These results may indicate a limitation to this often-used technique.

Therefore, experiments were conducted with different levels of phosphate charge: −0.4, −0.6, −0.8, and the standard level of −1. An energy minimization of the cisplatin molecule was performed as described above and then an exploratory dynamics trajectory as described below was undertaken with these different reduction levels. A charge of −0.6 per nucleotide was found to be the minimum requirement for maintenance of the basic major groove geometry observed in the crystal structure. Thus, a charge reduction of −0.6 was used for the remainder of the simulations, with specific point charges arranged in the manner described previously (Veal and Wilson, 1991; Table 2).

The cisplatin and oxaliplatin adduct starting structures were subjected to 1000 steps of steepest descent and 7000 steps of conjugate gradient energy minimization in the in vacuo conditions described above. At the conclusion of the minimization, the cisplatin structure had a RMS derivative of ~0.05 kcal $mol^{-1}Å^{-1}$. The oxaliplatin structure achieved convergence (maximum derivative <0.001 kcal $mol^{-1}Å^{-1}$) before the completion of the full 7000 conjugate gradient steps. The resultant structures were analyzed and also were used as starting structures for the molecular dynamics simulations.

As our cisplatin parameters had been initially been refined in a molecule with phosphate charges of −0.2, it was important to ensure that the changes made to the phosphate charges had not compromised the reliability of the forcefield values. A cisplatin molecule with phosphate charges of −0.2 was subjected to an identical minimization as described above, and the minimized forms of −0.2 and −0.6 phosphate-charged molecules compared. The shift in charge had a minimal effect on the structures, with a whole-molecule (heavy atom) RMS deviation of only 0.23Å. If only the platinum, amine

nitrogens, and heavy atoms of the two bound guanine bases were considered, RMS deviation was only 0.03Å.

Checked against the crystal structure, the energy-minimized cisplatin structure (with a −0.6 charge per nucleotide) still provided a reasonable model, with a whole-molecule (heavy atom) RMS deviation of 0.92Å. If only the platinum, amine nitrogens, and heavy atoms of the two bound guanine bases were considered, the RMS deviation was only 0.34Å, a value equivalent to that achieved in the initial parameter development stage. Thus, no adjustments were made to the platinum parameters from the values determined earlier in this study.

Molecular Dynamics. To search a larger conformational space and provide a structure less subject to the local minima often achieved during energy minimization, molecular dynamics simulations of the cisplatin- and oxaliplatin-adducted DNA models were performed with the Discover module of InsightII. All dynamics simulations were performed in the same in vacuo conditions and with the same parameters and charges as described above. The starting structures used were the energy-minimized forms described in the previous section. Exploratory dynamics trajectories were run at a constant temperature of 298°K for 200 ps after a 20-ps equilibration. A time step of 0.001 ps was used, and conformers were sampled every 0.05 ps. No cutoffs were used for nonbonded interactions.

Although the adjustment of the phosphate charges to −0.6 prevented closure of the major groove in the cisplatin molecule, the exploratory simulations were somewhat unstable. Irreversible base pair-opening events were observed in most simulations within the first 100 ps, leading to considerable degradation of the DNA structure, especially at the ends of the molecule. This sort of structure degradation can be dealt with by using force constraints to maintain hydrogen bond distances between base pairs in the molecule (Kozack and Loechler, 1997). However, this will enforce a set of base-pairing distances and geometries, and as our priority was to study the adduct at the center of the molecule, where some base pairings are distorted, a different, simpler scheme was chosen. The simulation was constrained by fixing the position of the terminal phosphorous atoms at the 5′ and 3′ ends of both strands. Although this arrangement reduced the amount of conformational space that could be sampled, it was sufficient to prevent base opening and provided insurance against degradation of the overall structure of the mole-

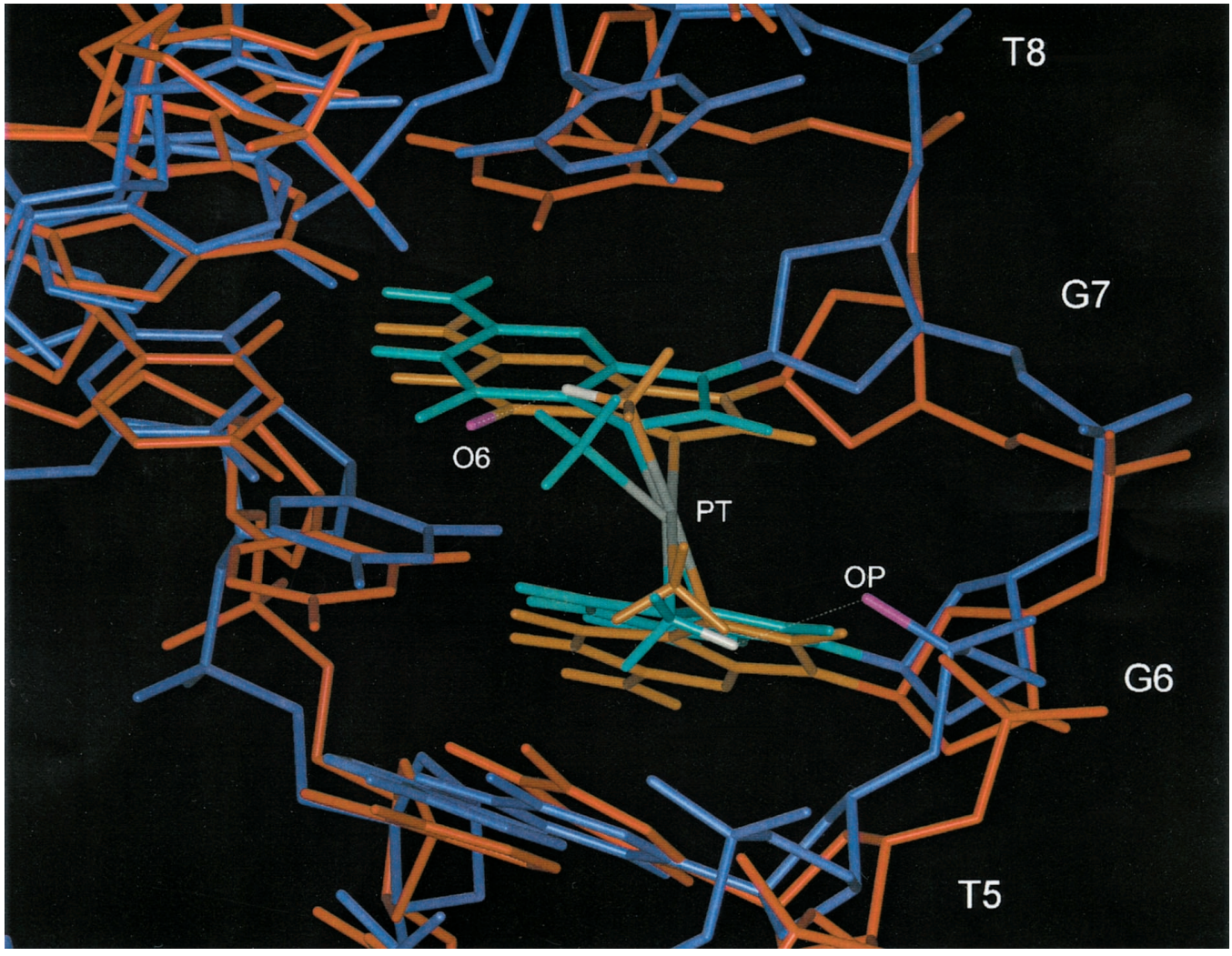

Fig. 5. View of the final modeled cisplatin adduct structure superimposed over the cisplatin adduct crystal structure. RMS deviation of heavy atoms was 1.37Å. The view faces the major groove, and is a close-up of the middle four base pairs of the dodecamer, with the cisplatin-bound guanine bases at the center. The ammine groups of cisplatin project outward toward the viewer. The cisplatin bound strand, on the right-hand side of the image, progresses from 3′ to 5′ from the top to the bottom of the image. This orientation was used for the adducted strand throughout this work to provide enhanced visual clarity. The bases on the adducted stand are labeled with type and sequence number. Hydrogens are only shown for the cisplatin adduct and two adducted guanines. Blue, overall cisplatin crystal structure. Cyan, two bound guanines and cisplatin adduct of crystal structure. Red, overall cisplatin final structure. Orange, two bound guanines and cisplatin adduct of final structure. Gray, platinum atom of cisplatin in both structures. Magenta, oxygen involved in H-bond with an ammine group. White, hydrogen involved in H-bond with oxygen. O6, guanine oxygen H-bonded to ammine hydrogen in final structure; OP, phosphate oxygen H-bonded to ammine hydrogen in crystal structure.

cule. Furthermore, because only two atoms at each end of the molecule were restrained, the adducts (located in the center of a reasonably long and flexible DNA molecule) were relatively free to move throughout the simulation. However, it should be noted that this arrangement, although permitting reasonable exploration of local adduct conformation, reduces the ability of the simulation to make predictions about global DNA changes brought on by the adducts.

Final dynamics trajectories were run at a constant temperature of 298°K for 500 ps after a 20-ps equilibration. A time step of 0.001 ps was used, and conformers were sampled every 0.05 ps. No cutoffs were used for nonbonded interactions. Among the resulting pool of 10,000 conformers, every fourth structure was sampled to produce a group of 2500 conformers. These structures were averaged through the Analysis module of InsightII. The resulting average structure was energy-minimized for 100 steepest descent steps without restraints to remove artifacts of the structure averaging procedure. The resultant structures were analyzed as the "final" cisplatin and oxaliplatin adduct structures.

Results

The Cisplatin Adduct Model. The final cisplatin structure predicted by the modeling process was compared with the crystal starting structure to validate the chosen parameters. The parameters proved to be a reasonable predictor of cisplatin complex behavior. If the overall structures were considered, RMS deviation (of heavy atoms) between the final cisplatin structure and the crystal structure was 1.37Å. If only the platinum, ammine nitrogens, and heavy atoms of the two bound guanine bases were considered, RMS deviation was 0.28Å, a value similar to those observed in the validation steps of Yao et al. (1994), and superior to the 0.34Å value that was achieved in the prior energy minimization step.

The final cisplatin adduct structure is shown superimposed over the crystal structure in Fig. 5. Although the structures exhibited a large degree of agreement, there were some differences between the modeled and crystal structures. The modeled structure exhibited an adduct with a square planar structure across the N32-PT-NB2 and N31-PT-NB1 bonds, whereas the crystal structure had a mildly bent geometry. However, the planar geometry is expected for cisplatin molecules, and was also observed in Yao et al. (1994), and other modeling studies of cisplatin (Kozelka and Chottard, 1990; Herman et al., 1990). As the 2.6Å resolution of the crystal structure (Takahara et al., 1996a,b) was not adequate to determine the exact position of the ammine and Pt atoms, the planar geometry observed in the current study is certainly not unreasonable.

The predicted hydrogen bonding pattern was also different. The crystal structure displayed an H-bond between the 5′ ammine (N31) hydrogen and one of the 5′ phosphate pendant oxygens. No H-bonds were present involving the 5′ ammine group in the final modeled structure. However, formation of such a bond is clearly not precluded in the modeled arrangement, as it was maintained in the energy minimized form before the molecular dynamics (MD) simulation. As the final modeled structure is an average of MD conformers, it will not necessarily display H-bond interactions that were achieved in particular sections of the simulation. Furthermore, such an H-bond was also not observed in the NMR solution structures (Yang et al., 1995; Gelasco and Lippard, 1998), suggesting that this interaction is not an essential characteristic of cisplatin adducts.

Conversely to the phosphate H-bond above, final modeled structure also displayed an H-bond that the crystal structure lacks. The 3′ ammine group (N32) hydrogen formed an H-bond with the O6 atom of G7. In the energy-minimized modeled structure (pre-MD), this ammine group was H-bonded to the O4 atom of T8. The variety of bonds seen in both ammine groups suggests that their H-bonds may be dynamic in a real system, interacting with multiple internal and solvent atoms.

One more notable divergence between the crystal and modeled structures was the position of thymine 8 (T8). In the crystal structure, this base opened outward into the major groove, resulting in irregular hydrogen bonds with its pairing base, adenine 17 (A17). In the final modeled structure, as well as in the energy-minimized structure, this base was rotated back into the helix to establish normal Watson-Crick base pairing (Fig. 5).

TABLE 3
Measurements of adduct angles in the final cisplatin and oxaliplatin modeled structures, defined by atom potential types as shown in Fig. 2

Angle	Cisplatin	Oxaliplatin
	degrees	*degrees*
Adduct "right" angles		
N32-PT-NB1	89.5	90.5
N31-PT-NB2	87.6	90.3
NB1-PT-NB2	92.3	91.1
N31-PT-N32	90.7	88.4
Angle	Cisplatin	Oxaliplatin
	degrees	*degrees*
Adduct "planar" angles		
NB1-PT-N31	177.4	175.9
NB2-PT-N32	177.5	176.6
Angle	Cisplatin	Oxaliplatin
	degrees	*degrees*
Base "roll" angles (relative to PT)		
N*-NB1-PT	155.0	156.6
N*-NB2-PT	142.3	143.4
CB-NB1-PT (C4-N7-PT)	158.0	159.5
CB-NB2-PT (C4-N7-PT)	139.9	143.6

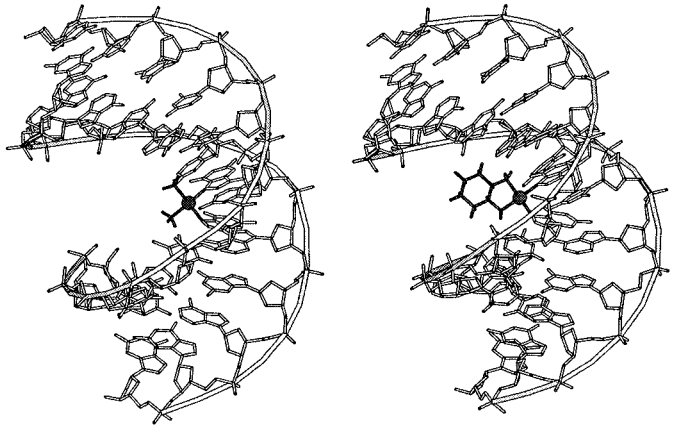

Fig. 6. MOLSCRIPT (Kraulis, 1991) image of the cisplatin and oxaliplatin final modeled structures shown in the same orientation (sideways with respect to the plane of the adducts). The adducted strand proceeds 3′ to 5′ from the top to the bottom of the image. A ribbon traces the phosphate backbone of each DNA strand. Both adducts (the darkened portions of the molecules) can be seen to protrude outward into the major groove. The platinum atom is rendered as a small sphere. Hydrogens are only shown for the drug adducts.

The above findings indicate that the platinum parameters and experimental environment selected produced a reasonable model of the cisplatin adduct structure. Although some differences were apparent, many were in interactions that were variable and not essential components of cisplatin adduct structure. The most important aspect of the model, the specific geometry of the cisplatin adduct and the bound guanine bases, was rendered with a high degree of fidelity by the developed parameters. Thus, we compared the modeled oxaliplatin and cisplatin structures to look for structural differences that might account for differential recognition of these adducts.

The Oxaliplatin Adduct Model. Overall, the cisplatin and oxaliplatin final structures exhibited a great degree of similarity. If the cyclohexane ring was disregarded and RMS deviation between the two molecules calculated, the differences were minimal. The RMS deviation between the heavy atoms of the entire molecules was 0.98Å, a value less than that for the cisplatin final modeled structure versus the crystal structure. When only the Pt, ammine/amine nitrogen, and heavy guanine atoms were considered, the RMS deviation was 0.07Å.

Although the adduct structures were very similar, the presence of the oxaliplatin cyclohexane ring, which maintained the expected "chair" conformation, did have a mild effect on the adduct geometry. The N31-PT-N32 and NB1-PT-NB2 angles were decreased, and the N31-PT-NB2 and N32-PT-NB1 angles were increased, as shown in Table 3. Furthermore, base roll relative to the platinum atom was increased as measured by the N*-NBX-PT (N9-N7-PT) and CB-NBX-PT (C4-N7-PT) angles. The oxaliplatin structure exhibited the same square-planar geometry as the cisplatin structure, although the cyclohexane residue appeared to reduce the planarity of the complex mildly. The NB1-PT-N31 and NB2-PT-N32 angles were reduced from complete planarity (180°) to a greater degree than those in cisplatin (Table 3).

Other features described above for the final modeled cisplatin structure, such as the lack of H-bonding between the 5′ amine (N31) and a 5′ phosphate oxygen and the restoration of Watson-Crick base pairing at T8, were maintained in the final modeled oxaliplatin structure. However, the oxaliplatin adduct displayed a different hydrogen bonding pattern at the 3′ amine (N32). A hydrogen from this group was H-bonded to the O4 atom of thymine 8, an arrangement seen in both the cisplatin and oxaliplatin energy-minimized (pre-MD) structures. It is possible that the cyclohexane residue promoted retention of this bond during the MD simulation through the limitation it imposed on the rotation of the amine groups.

It is unclear whether the mild deviations in the immediate adduct structure between the cisplatin and oxaliplatin models are a result of direct effects of the cyclohexane residue or indirect (nonbonded) effects that have been translated through the DNA strand to the two bound guanine bases. The fact that the RMS deviation was so low between the two immediate adduct structures (0.07Å), yet much higher between the overall structures (0.98Å), suggested that the primary mode of the differential effect of oxaliplatin on the DNA structure might be nonbonded interactions between the cyclohexane residue and the DNA strands.

As explained in the discussion of the molecular dynamics methodology, restraints placed on the terminal phosphates reduce the capability of the simulation to comment on the relative global DNA effects produced by oxaliplatin and cisplatin. However, as the molecules were completely unrestrained during the energy minimization step, and only partially restrained during the dynamics simulation, several interesting observations about global structural differences can be made. As shown in Fig. 6, the overall DNA configuration was similar for cisplatin and oxaliplatin. Although the structures displayed minimal divergence, there was a narrowing of the major groove in the oxaliplatin final structure relative to the cisplatin final structure. Following a method previously described (Falsafi and Reich, 1993), the major groove width was measured as the distance between the phosphate group of one nucleotide and the phosphate group of its closest neighbor across the groove (this nucleotide was five to six steps down the helix from the first in our molecules). Measured in this way, the average major groove width was 14.2 ± 2.3 Å in the cisplatin molecule but only 12.2 ± 0.8 Å in the oxaliplatin molecule (similar to the crystal structure width of 11.7 ± 1.4 Å) The narrowed major groove suggests the possibility of a more A-DNA-like conformation in the case of oxaliplatin.

Minor groove width was measured in a similar manner, with the closest neighbor phosphate across the minor groove being three steps down the helix. As demonstrated by the data presented in Table 4, the width was very similar, averaging 13.1 ± 1.5 Å in the cisplatin molecule and 13.2 ± 1.4 Å in the oxaliplatin molecule. Average width in the crystal structure was larger at 15.2 ± 1.0 Å. Both models retained a similar minor groove width to that of the crystal structure in the region of the helix containing the platinum-bound G6 and G7. However, the groove quickly narrows as one proceeds away from the adduct. This suggests a more B-DNA-like character to the modeled cisplatin and oxaliplatin molecules relative to the cisplatin crystal structure.

Sugar puckers in both molecules were primarily of the unusual O4′-endo conformation, most likely as an artifact of the averaged MD structure. δ angles of the DNA backbone were almost entirely in the range of 105–130°, higher than the angle for the C3′-endo pucker of canonical A-DNA (~85°) and lower than the angle for the C2′-endo pucker of canonical B-DNA (~155°; canonical angles as given by Takahara et al., 1996b). This prevented a meaningful comparison of the sugar-pucker types (and their A-DNA- or B-DNA-like character) in the modeled cisplatin and oxaliplatin adducts. The degree

TABLE 4
Minor groove widths, measured as the distance between one phosphate and its nearest neighbor across the groove three phosphates down the helix

Phosphate Pair	Cisplatin Crystal	Cisplatin Model	Oxaliplatin Model
	Å	Å	Å
C4-G24	15.4	12.7	12.4
T5-G23	15.7	13.9	14.0
G6-A22	15.8	15.1	15.2
G7-G21	16.8	15.6	15.3
T8-A20	15.9	13.2	13.8
C9-C19	14.7	12.1	12.5
T10-C18	15.1	12.1	12.3
C11-A17	14.4	11.9	12.1
C12-G16	13.5	11.5	11.6
Average	15.2	13.1	13.2
S.D.	1.0	1.5	1.4

of bend of the oxaliplatin and cisplatin final structures was not quantified, but by visual inspection, there was very little divergence from the bend observed in the crystal structure for either cisplatin or oxaliplatin.

As shown in Figs. 6 and 7, the most distinctive difference between the final modeled structures of oxaliplatin and cisplatin remained the cyclohexane ring present in the oxaliplatin adduct. The ring protruded an additional 3.7Å into the major groove relative to cisplatin. The cyclohexane "chair" conformation was apparently accommodated well by the square planar geometry of the platinum and nitrogen groups, and it protruded directly outward in the plane described by

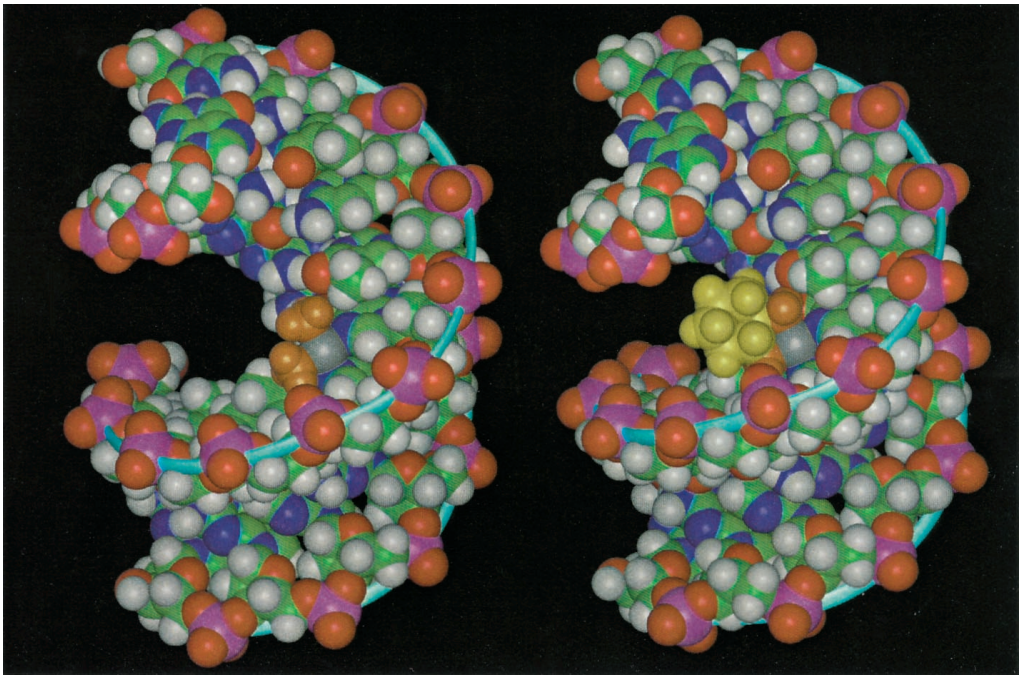

Fig. 7. Space-filling view of the cisplatin (left) and oxaliplatin (right) final modeled structures in the same orientation as in Fig. 6. The DACH ring of oxaliplatin can be seen to fill much of the major groove. A cyan ribbon traces the phosphate backbone of each DNA strand. Green, carbon. Purple, nitrogen. Red, oxygen. White, hydrogen. Magenta, phosphorous. Gray, platinum. Orange, ammine/amine nitrogen and hydrogens. Yellow, cyclohexane ring of oxaliplatin.

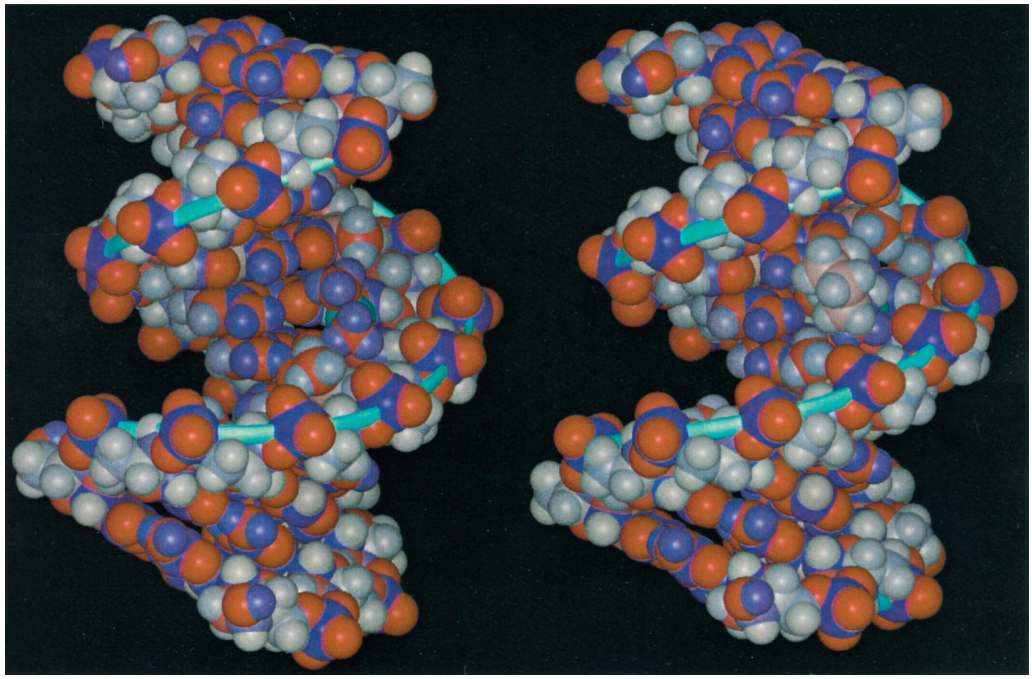

Fig. 8. Space-filling view of the cisplatin (left) and oxaliplatin (right) final modeled structures colored by atom according to partial charge. Coloration is on a sliding scale, with shades of purple denoting positive charge, white denoting neutral, and shades of red denoting negative charge. Dark purple indicates charge ≥ 0.5, and dark red indicates charge ≤ -0.5. Atoms with charges between these extremes are shaded the appropriate lightened color as they approach neutrality (white). The molecules are rotated approximately 90° around the helical axis from the image presented in Fig. 7, such that the viewer is facing the major groove and the platinum adducts. The two adducts sit slightly to the right of the middle of the two molecules. The platinum atom is colored cyan (it would be dark purple if colored on the basis of its charge) and is visible in the cisplatin molecule but only slightly visible in the oxaliplatin molecule. The phosphate backbone is traced by a cyan ribbon to clarify the groove structure. The area between the two ribbons, in which the adducts are situated, is the major groove. The area above and below the ribbons is the minor groove. The mild major groove narrowing in the oxaliplatin molecule can be discerned visually. The polar cisplatin adduct and the polar DNA region around it can be clearly discerned as an area of red and purple atoms. The oxaliplatin cyclohexane ring can be seen to sit within this region, a distinctly nonpolar (white and pink) molecule.

these atoms. Angle measurements across the NB1/N32/CT (cyclohexane) and NB2/N31/CT angles yielded near-planar results, within the limits of the uneven cyclohexane ring, of ~170°. In the space-filling model presented in Fig. 7, the cyclohexane ring can be seen to fill much of the narrowed major groove.

Discussion

The molecular modeling results presented here suggest that cisplatin and oxaliplatin produce similar effects on DNA structure. This is particularly true for the covalent effects of the two drugs. The marked similarity in the geometry of the shared cisplatin and oxaliplatin adduct bonds in our models indicates that the cisplatin adduct geometry is likely to be capable of absorbing the stresses introduced by the cyclohexane residue of oxaliplatin without significant distortion.

However, the results do suggest a mild effect of the cyclohexane residue of oxaliplatin on the major groove structure. Our preliminary work, with a phosphate-charge reduction to −0.2 per nucleotide, demonstrated a severe tendency for major groove narrowing relative to cisplatin on energy minimization. Although this simulation was unstable, work with a more stable system (with a phosphate charge reduction to −0.6 per nucleotide) still displayed a more narrow major groove in the oxaliplatin molecule than in the cisplatin molecule. This may suggest oxaliplatin has different effects on the larger DNA structure, perhaps a tendency toward a more A-DNA-like helix. Although a broadened range of conformational space was searched with the molecular dynamics simulations, the fact that constraining of the terminal phosphorous atoms was necessary to stabilize the helix prevented a complete survey of potential helical conformations. Therefore, the possibility that the DACH ring of oxaliplatin produces a more dramatic shift in overall DNA conformation through nonbonded interactions cannot be excluded.

Because the adducted portions of the molecules were subject to the greatest degree of conformational search, the refined parameters for the Pt and other adduct atoms were also maximally tested. The parameters for Pt and its interacting atoms were quite successful at reproducing the cisplatin adduct within the context of a full-length double- stranded molecule. Although some aspects of the overall molecule and its interactions with the adduct atoms, such as H-bonding, differed from those of the crystal structure, many of these interactions appear to be highly dynamic. Others, such as the rotation of T8 to establish standard H-bonding, may be more a result of the features of the AMBER field than the introduced parameters and may represent corrections of peculiarities in the crystal structure brought on by packing forces.

As this study was nearing completion, the NMR solution structure of an essentially identical cisplatinated DNA molecule to the one solved crystallographically (and used here) became available (Gelasco and Lippard, 1998). Although this structure displayed the same overall features as the crystal structure, it also differed with respect to specific aspects of the geometry, most notably a larger helical bend and some increase in base roll at the site of the adduct (Gelasco and Lippard, 1998). When compared with the crystal structure in the form used in this study, the NMR structure displays a whole-molecule, heavy-atom RMS deviation of 5.27 Å. If only the platinum, ammine nitrogens, and heavy atoms of the two bound guanine bases are considered, RMS deviation is still a notable 1.22 Å. The final cisplatin model presented here yields essentially identical results when compared with the NMR structure, with RMS deviation measurements of 5.29 and 1.20 Å, respective to the above. As the crystal structure was used as the basis for the cisplatin model, it is not surprising that both structures compare similarly to the NMR results. However, it is interesting to note that relative to the changes seen in these two experimentally derived cisplatin structures, the changes observed here between the cisplatin and oxaliplatin models can be considered to be extremely small.

A complete examination of the overall effects on DNA structure of oxaliplatin adduct formation may become possible in the future through the use of full solvent, explicit counter-ions, and the particle mesh Ewald summation for the treatment of boundary conditions. Recently, this method has been shown to provide simulations in which the stability of the DNA helix was retained, and very reasonable structures produced, in DNA molecules (Young et al., 1997; Duan et al., 1997). As these studies are expanded into the area of platinum drug adducts, we offer the cisplatin and oxaliplatin parameters refined and developed in this study.

Although cisplatin and oxaliplatin produced only small differences in the structure of the DNA itself, the presence of the DACH ring in oxaliplatin resulted in a large difference in adduct structure. The modeling indicates that the DACH ring projects directly outward into the major groove, filling much of the available space near the two bound guanines. Not only is the DACH group bulky relative to ammines of cisplatin (Fig. 7), Fig. 8 shows that it is electrostatically distinct due to its nonpolar character. The adducts of both drugs reside in a portion of the DNA molecule populated by polar groups and hydrogen bond donors/acceptors. The polar ammine groups of the cisplatin adduct match this environment nicely, but the nonpolar cyclohexane group does not. The two amine groups of oxaliplatin and portions of the other polar groups are partially hidden behind the cyclohexane residue in the oxaliplatin adduct. This configuration would surely present a very distinct “binding pocket” to proteins of the mismatch repair system and any other DNA-binding proteins that might require interactions with the major groove.

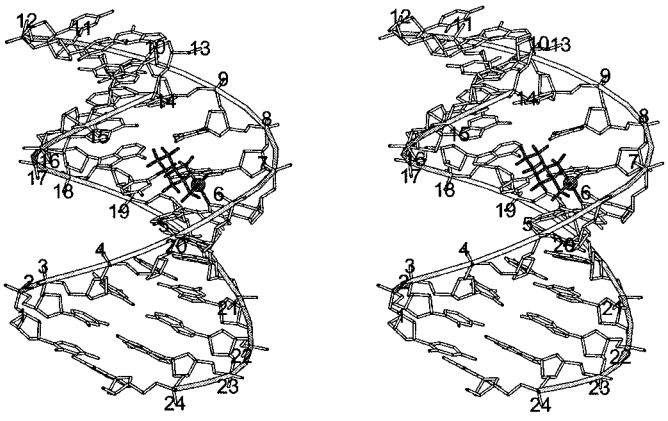

Fig. 9. MOLSCRIPT (Kraulis, 1991) stereo view of the oxaliplatin adduct final modeled structure, with the numbering scheme of the nucleotides. The molecule is in approximately the same orientation as in Fig. 8 with the DACH ring projecting outward toward the viewer from the major groove.

The presence of the DACH ring in the major groove may be sufficient to explain the differential treatment cisplatin and oxaliplatin adducts apparently receive from the MMR system. Both hMSH2 (Mello et al., 1996) and the heterodimer of hMSH2 and hMSH6 (Yamada et al., 1997) bind to cisplatin adducts. The normal function of the hMSH2/hMSH6 dimer is to bind to mispaired bases and single base loops. Single or double base mispairs produce very slight perturbations in DNA structure (Hunter et al., 1986; Prive et al., 1991) that may be mimicked by the projecting ammine groups of cisplatin. Additionally, some single base loops can produce helical bends in DNA (Turner, 1992) and the bend produced by the cisplatin adduct may also mimic this structure. This mimicry is thought to be the basis for recognition of cisplatin adducts by the MMR system. The cisplatin adducts may be sufficiently similar to true mismatches to attract the MMR proteins, but sufficiently unique to be improperly processed by the system or bound so tightly that appropriate repair systems cannot be engaged. In any event, the cyclohexane residue present in oxaliplatin adducts is well positioned to prevent this binding through both its bulkiness and nonpolar character. Figure 9 provides a stereoview of the modeled oxaliplatin structure.

Even if, despite steric hindrance by the DACH ring, the hMSH2/hMSH6 heterodimer could bind to oxaliplatin adducts, the presence of the ring might alter the ability of the MMR complex to process the adduct due to structural differences in the DNA itself. The modeling suggested that the DACH ring promotes narrowing of the major groove, and perhaps a more A-DNA-like conformation to the helix. This conformation change, alone or when coupled to the bulky DACH adduct, might provide a distortion that is distinct enough to alter processing.

The lack of a crystal structure for hMSH2 or any other MMR protein limits speculation on the specific role of the DACH ring of oxaliplatin in the differential MMR response to oxaliplatin adducts relative to cisplatin adducts. However, information on the binding of the bacterial MutS protein (Biswas and Hsieh, 1997) suggests that MMR proteins contact mismatches at multiple points along the major and minor grooves near the adduct, as well as contacting the adduct directly. Thus, it is possible that both adduct structure and the drug-induced changes in overall DNA conformation modulate MMR protein binding. We offer the modeled oxaliplatin adduct structure as a tool with which to investigate this issue further.

Acknowledgments

We thank Molecular Simulations, Inc. (MSI) for providing software licenses to the San Diego Supercomputer Center in support of molecular modeling classes in which this research was initiated, and the San Diego Supercomputer Center for computer time and facilities support for this work. We also thank Roberto Lins for helpful discussions and suggestions, Celeste Lashley for assistance with computing issues, and John Tate for help in preparing the MOLSCRIPT figures.

References

Bernstein FC, Koetzle TF, Williams GJ, Meyer EF Jr, Brice MD, Rodgers JR, Kennard O, Shimanouchi T and Tasumi M (1977) The Protein Data Bank: A computer-based archival file for macromolecular structures. *J Mol Biol* **112:** 535–542

Biswas I and Hsieh P (1997) Interaction of MutS Protein with the Major and Minor Grooves of a Heteroduplex DNA. *J Biol Chem* **272:**13355–13364.

De las Alas MM, de Bruin RAM, Ten Eyck L, Los G and Howell SB (1998) Prediction-based threading of hMSH2 DNA mismatch repair protein. *FASEB J* **12:**653–663.

Duan Y, Wilkosz P, Crowley M and Rosenberg JM (1997) Molecular dynamics simulation study of DNA dodecamer d(CGCGAATTCGCG) in solution: Conformation and hydration. *J Mol Biol* **272:**553–572.

Falsafi S and Reich NO (1993) Molecular dynamics simulations of B-DNA: An analysis of the role of initial molecular configuration, randomly assigned velocity distribution, long integration times, and nonconstrained termini. *Biopolymers* **33:**459–473.

Fink D, Nebel S, Aebi S, Zheng H, Cenni B, Nehme A, Christen RD and Howell SB (1996) The role of DNA mismatch repair in platinum drug resistance. *Cancer Res* **56:**4881–4886.

Gelasco A and Lippard SJ (1998) NMR solution structure of a DNA dodecamer duplex containing a *cis*-diammineplatinum(II) d(GpG) intrastrand cross-link, the major adduct of the anticancer drug cisplatin. *Biochemistry* **37:**9230–9239.

Herman F, Kozelka J, Stoven V, Guittet E, Girault J-P, Huynh-dinh T, Igolen J, Lallemand J-Y and Chottard J-C (1990) A d(GpG)-platinated decanucleotide duplex is kinked. An extended NMR and molecular mechanics study. *Eur J Biochem* **194:**119–113.

Hunter WN, Brown T, Anand NN and Kennard O (1986) Structure of an adenine-cytosine base pair in DNA and its implications for mismatch repair. *Nature (Lond)* **320:**552–555.

Kozack RE and Loechler EL (1997) Molecular modeling of the conformational complexity of (+)-*anti*-B[*a*]PDE-adducted DNA using simulated annealing. *Carcinogenesis* **18:**1585–1593.

Kozelka J and Chottard J-C (1990) How does cisplatin alter DNA structure? A molecular mechanics study on double-stranded oligonucleotides. *Biophys Chem* **36:**165–178.

Kraulis PJ (1991) MOLSCRIPT: A program to produce detailed and schematic plots of protein structure. *J Appl Crystallogr* **24:**946–950.

Mello JA, Acharya S, Fishel R and Essigmann JM (1996) The mismatch-repair protein hMSH2 binds selectively to DNA adducts of the anticancer drug cisplatin. *Chem Biol* **3:**579–589.

Orozco M, Laughton CA, Herzyk P and Neidle S (1990) Molecular-mechanics modelling of drug-DNA structures; the effects of differing dielectric treatment on helix parameters and comparison with a fully solvated structural model. *J Biomol Struct Dyn* **8:**359–373.

Prive GG, Yanagi K and Dickerson RE (1991) Structure of the B-DNA decamer C-C-A-A-C-G-T-T-G-G and comparison with isomorphous decamers C-C-A-A-G-A-T-T-G-G and C-C-A-G-G-C-C-T-G-G. *J Mol Biol* **217:**177–199.

Raymond E, Faivre S, Woynarowski JM and Chaney SG (1998) Oxaliplatin: Mechanism of action and antineoplastic activity. *Semin Oncol* **25(Suppl 5):**4–12.

Saris CP, van de Vaart PJM, Rietbroek RC and Blommaert FA (1996) In vitro formation of DNA adducts by cisplatin, lobaplatin, and oxaliplatin in calf thymus DNA in solution and in cultured human cells. *Carcinogenesis* **17:** 2763–2769.

Scheeff ED and Howell SB (1998) Computer modeling of the primary cisplatin and oxaliplatin DNA adducts and relevance to mismatch repair recognition (Abstract). *Proc Am Assoc Cancer Res* **39:**158.

Takahara PM, Frederick CA and Lippard SJ (1996a) Crystal structure of the anticancer drug cisplatin bound to duplex DNA. *J Am Chem Soc* **118:**12309–12321.

Takahara PM, Rosenzweig AC, Frederick CA and Lippard SJ (1996b) Crystal structure of double-stranded DNA containing the major adduct of the anticancer drug cisplatin. *Nature (Lond)* **377:**649–652.

Turner DH (1992) Bulges in nucleic acids. *Curr Opin Struct Biol* **2:**334–337.

Veal JM and Wilson WD (1991) Modeling of nucleic acid complexes with cationic ligands: A specialized molecular mechanics forcefield and its application. *J Biomol Struct Dyn* **8:**1119–1145.

Weiner SJ, Kollman PA, Case DA, Singh UC, Ghio C, Alagona G, Profeta J and Weiner P (1984) A new force field for molecular mechanical simulation of nucleic acids and proteins. *J Am Chem Soc* **106:**765–784.

Woynarowski JM, Chapman WG, Napier C, Herzig MCS and Juniewicz P (1998) Sequence- and region- specificity of oxaliplatin adducts in naked and cellular DNA. *Mol Pharmacol* **54:**770–777.

Yamada M, O'Regan E, Brown R and Karran P (1997) Selective recognition of a cisplatin-DNA adduct by human mismatch repair proteins. *Nucl Acids Res* **25:** 491–495.

Yang D, van Boom SSGE, Reedijk J, van Boom JH and Wang AHJ (1995) Structure and isomerization of an intrastrand cisplatin-cross-linked octamer DNA duplex by NMR analysis. *Biochemistry* **34:**12912–12920.

Yao S, Plastaras JP and Marzilli LG (1994) A molecular mechanics AMBER-type force field for modeling platinum complexes of guanine derivatives. *Inorg Chem* **33:**6061–6077.

Young MA, Ravishanker G and Beveridge DL (1997) A 5-nanosecond molecular dynamics trajectory for B-DNA: Analysis of structure, motions, and solvation. *Biophys J* **73:**2313–2336.

Send reprint requests to: Stephen B. Howell, M.D., Department of Medicine 0058, UCSD Cancer Center, University of California, San Diego, 9500 Gilman Dr., La Jolla, CA 92093-0058. E-mail: showell@ucsd.edu